A Letters Journal Exploring the Frontiers of Physics

December 2013

EPL, **104** (2013) 69002
doi: 10.1209/0295-5075/104/69002

www.epljournal.org

Energy transfers during dynamo reversals

Pankaj Mishra[1], Christophe Gissinger[1], Emmanuel Dormy[2] and Stephan Fauve[1]

[1] *Laboratoire de Physique Statistique, Ecole Normale Supérieure, CNRS, Université P. et M. Curie, Université Paris Diderot - Paris, France*
[2] *MAG(CNRS/ENS/IPGP), LRA, Ecole Normale Supérieure - Paris, France*

received 19 September 2013; accepted in final form 9 December 2013
published online 10 January 2014

PACS 91.25.Cw – Origins and models of the magnetic field; dynamo theories
PACS 47.65.-d – Magnetohydrodynamics and electrohydrodynamics

Abstract – Using direct numerical simulations of the equations of magnetohydrodynamics, we study reversals of the magnetic field generated by the flow of an electrically conducting fluid in a sphere. We show that at low magnetic Prandtl numbers, $Pm = 0.5$, the decrease of magnetic energy, ohmic dissipation and power of the Lorentz force during a reversal is followed by an increase of the power injected by the force driving the flow and an increase of viscous dissipation. Cross correlations show that the power of the Lorentz force is in advance with respect to the other energy flows. We also observe that during a reversal, the maximum of the magnetic energy density migrates from one hemisphere to the other and comes back to its initial position, in agreement with recent experimental observations. For larger magnetic Prandtl numbers ($Pm = 1, 2$), the magnetic field reversals do not display these trends and strongly differ one from another.

Introduction. – It has been known since the work of Brunhes that the dipolar component of the magnetic field of the Earth has changed sign in a random way on geologic time scale [1]. It is now believed that the Earth magnetic field is generated by a dynamo process, *i.e.* an instability related to electromagnetic induction by the flow of liquid iron in the Earth's core [2]. In the past 50 years, many models of reversals of the magnetic field have been elaborated using various concepts and methods of fluid dynamics and dynamical system theory [3]. Although reversals are occurring randomly, a strong emphasis has been put on identifying patterns in the flow that generate them and thus could be considered as precursors. Parker first proposed two possible scenarios: the first one was related to the fluctuations of the number and positions of cyclonic convective cells in the core [4]. The second one, based on a temporary weakening of the meridional circulation [5], was indeed observed later in numerical simulations [6].

Direct simulations of the magnetohydrodynamics (MHD) equations in a rotating sphere that display reversals of magnetic field have been achieved since 1995 [7]. Besides Parker's mechanism, other flow patterns have been identified as possible precursors of reversals, such as convective plumes locally producing a magnetic field with opposite polarity [8]. In more recent numerical simulations of the geodynamo, a stronger emphasis has been put on typical patterns of the magnetic field rather than the velocity field as possible precursors of field reversals [9]. Note however that these simulations have been conducted at high values of Pm (mostly in the range 10 to 20) and that it has been shown that the geometry of the magnetic field and its reversals strongly depend on the parameter values of these geodynamo numerical models [10]. On the one hand, no simple general pattern seemed to emerge since successive reversals in a given simulation can look different one from the other, but on the other hand, several simulations showed that the flow symmetries are playing an important role. The emission of poleward light plumes identified as a precursor of reversals [6,8], breaks the equatorial symmetry of the flow in the liquid core. Breaking north-south symmetry of the convection pattern has been indeed found to be a necessary condition for reversals in some geodynamo numerical models [11].

This last feature has also been observed in a laboratory experiment involving a von Karman swirling flow of liquid sodium driven by two coaxial propellers in a cylinder (the VKS experiment). With propellers counter-rotating at the same speed, only stationary dynamos are generated whereas counter-rotation at different speeds yields time-dependent regimes including random reversals [12]. It has been shown that the symmetry broken by rotating the propellers at different speeds allows a linear coupling between dipolar and quadrupolar modes of the magnetic field that provides a model for field reversals [13].

Direct simulations of the MHD equations with a similar flow forcing in a spherical geometry display the same features [14].

Broken symmetries of the flow, either occurring spontaneously as in the geodynamo, or externally induced as in the VKS experiment, thus play an important role in the observation of regimes involving reversals of the magnetic field. The aim of this work is to identify characteristic patterns of reversals with the help of numerical simulations. Instead of looking at patterns of the velocity or magnetic fields, we look at the behavior of energy transfers within the system during the process of field reversal. After recalling the governing equations, we will show how the energy flow between the velocity and magnetic field, *i.e.* the power of the Lorentz force, is correlated with ohmic and viscous dissipation as well as with the injected power by the forces driving the flow. We will then study the behavior of these energy transfers during reversals of the magnetic field.

Governing equations and simulation details. – The MHD equations are numerically integrated in a spherical geometry for the solenoidal magnetic $\mathbf{b}(r,\theta,\phi)$ and velocity $\mathbf{u}(r,\theta,\phi)$ fields

$$\frac{\partial \mathbf{u}}{\partial t} + Rm_0(\mathbf{u}\cdot\nabla)\mathbf{u} = -Rm_0\nabla\pi + Pm\Delta\mathbf{u} + Rm_0\mathbf{f} + Rm_0\left(\mathbf{b}\cdot\boldsymbol{\nabla}\right)\mathbf{b}, \quad (1)$$

$$\frac{\partial \mathbf{b}}{\partial t} = Rm_0\nabla\times(\mathbf{u}\times\mathbf{b}) + \Delta\mathbf{b}. \quad (2)$$

The above equations have been made dimensionless by using the radius of the sphere a as length scale and the magnetic diffusion time, $\tau_0 = \mu_0\sigma a^2$ as time scale. μ_0 is the magnetic permeability and σ is the electrical conductivity. $Pm = \mu_0\sigma\nu$ is the magnetic Prandtl number where ν is kinematic viscosity. π is the pressure field. The applied force is $\mathbf{f}(s,\phi,z)$ where, $f_\phi = s^2\sin(\pi s b)$, $f_z = \epsilon\sin(\pi s c)$ for $z>0$ and equal magnitude but opposite sign for $z<0$. Polar coordinates (s,ϕ,z) normalized by a, are used for the representation of the forcing term. In order to simulate finite sized impellers, this forcing is restricted to the region $0.25a < |z| < 0.65a$ and $s < s_0$. Here, $s_0 = 0.4$, $b^{-1} = 2s_0$, and $c^{-1} = s_0$. This forcing term and non-dimensional form have both previously been used to model both the Madison [15] and the VKS experiments [14,16]. It is invariant by a rotation of an angle π along any axis in the midplane (herafter called the R_π symmetry). In order to reproduce the magnetic field reversals observed in the VKS experiment, which only occur when the counter-rotating impellers have different rotation rates, the R_π symmetry in our simulations is broken by considering a forcing of the form $C\mathbf{f}$, where C is an asymmetry parameter fixed to $C=1$ for $z<0$ but can be different from one for $z>0$. A typical velocity V_0 is used to define the input parameter $Rm_0 = \mu_0\sigma a V_0$. The magnetic Reynolds number is $Rm = \max(u)Rm_0$ and the kinetic Reynolds number is $Re = Rm/Pm$.

The above system of equations is solved using the Parody numerical code [17], originally developed for the geodynamo and modified to make it suitable for configurations that involve a mechanical forcing of the flow.

We have performed simulations for different values of Pm and C. Depending on the value of these parameters, different dynamical regimes can be observed. For instance, when $Pm = 0.5$, a transition from a statistically stationary axial dipolar magnetic field to chaotic reversals is observed for $C \geq 1.5$, in agreement with the numerical observations reported in [14].

Energy budget. – Equations (1), (2) are used to obtain equations for the magnetic energy and the kinetic energy:

$$\frac{\mathrm{d}E^u}{\mathrm{d}t} = P - L - D^u, \quad (3)$$

$$\frac{\mathrm{d}E^b}{\mathrm{d}t} = L - D^b, \quad (4)$$

where, $E^u = 1/2\langle|\mathbf{u}|^2\rangle_V$ and $E^b = 1/2\langle|\mathbf{b}|^2\rangle_\infty$ are, respectively, the total kinetic and magnetic energy, $P = Rm_0\langle\mathbf{u}\cdot\mathbf{f}\rangle_V$ is the injected power, $L = -Rm_0\langle\mathbf{u}\cdot[(\boldsymbol{\nabla}\times\mathbf{b})\times\mathbf{b}]\rangle_V$ is the power of the Lorentz force, $D^u = -Pm\langle\mathbf{u}\cdot\Delta\mathbf{u}\rangle_V$ is the viscous dissipation, and $D^b = -\langle\mathbf{b}\cdot\Delta\mathbf{b}\rangle_V$ is the ohmic dissipation. In the above $\langle\cdot\rangle_V$ denotes spatial average over the sphere.

Equation (3) expresses that the rate of change of the kinetic energy is equal to the difference between the power injected by the driving force and the combined kinetic energy loss due to both the viscous dissipation and the power of the Lorentz force L. L is here defined such that $L>0$ corresponds to a positive transfer of energy from the velocity field to the magnetic field. Equation (4) shows that the rate of change of the magnetic energy is the difference between L and D^b. Therefore, L acts as a source term for the magnetic energy.

The mean values of the energies and powers that have been computed for different values of the governing parameters are reported in table 1. Several observations can be made. First, note that in all our runs, the ratio between the kinetic and the magnetic energy is always greater than one, and seems to be controlled by the magnetic Reynolds number, or more exactly by the distance from dynamo onset $Rm - Rm_c$, where Rm_c is the dynamo onset. Indeed, for a fixed value $Pm = 0.5$, this ratio increases as Rm is decreased, E^u and E^b being of the same order of magnitude when Rm is much larger than Rm_c. In most of the runs, the main part of the injected power is dissipated by viscosity, as the ratio D^u/D^b is generally greater than 1.5. D^b/D^u increases as Rm or Pm are increased.

Global energy balances have already been used to analyze geodynamo models [18] but mostly in statistically stationary regimes. The emphasis will be placed here on fluctuations of the energy transfers and their correlations, in particular during field reversals.

Table 1: Space and time averaged values of injected power (P), viscous (D^u) and ohmic (D^b) dissipations, power of the Lorentz force (L), kinetic (E^u) and magnetic (E^b) energies for different values of Pm and the asymmetry parameter C. For $Pm = 0.5$, the injected power increases with C, whereas the ratio of kinetic to magnetic energy decreases.

Pm	C	Rm_0	Re	P	D^u	D^b	L	E^u	E^b	E^u/E^b	D^u/P	D^b/P
0.5	1	300	230	3.99	3.44	0.59	0.588	0.0469	0.0028	16.8	0.86	0.14
	1.05	300	240	4.09	3.48	0.62	0.62	0.0469	0.0029	16.2	0.85	0.15
	1.25	300	237	4.46	3.68	0.78	0.78	0.0478	0.0036	13.3	0.82	0.18
	1.5	330	280	5.60	4.66	1.04	1.03	0.0591	0.0046	12.9	0.83	0.17
	2.0	390	370	8.17	6.24	2.06	2.05	0.0695	0.0331	2.1	0.76	0.25
1.0	2.0	700	400	15.32	10.86	4.78	4.73	0.0620	0.0142	4.4	0.70	0.30
2.0	2.0	1000	320	21.11	12.61	8.60	8.59	0.0369	0.0260	1.4	0.60	0.40

Although the flow is driven by a constant force, all the spatially averaged quantities involved in the energy budget (eqs. (3), (4)) fluctuate in time since both the velocity and magnetic fields are chaotic. We consider the cross correlation functions between these quantities in order to get some insight on their fluctuations. The cross correlation between two variables X and Y is defined as $C^{XY}(\tau) = \langle (X(t) - \bar{X})(Y(t+\tau) - \bar{Y})/\sigma_X \sigma_Y \rangle$, where ${\sigma_X}^2 = \overline{(X^2(t) - \bar{X}^2)}$, and ${\sigma_Y}^2 = \overline{(Y^2(t) - \bar{Y}^2)}$ are the variance of X and Y, respectively. $\bar{X}$ and $\bar{Y}$ represent mean values. The cross correlation functions between all the terms in eqs. (3), (4) computed from our numerical simulations are shown in fig. 1.

We first observe that purely kinetic quantities, P, D^u and E^u (not displayed), are well correlated, the maximum of the cross correlation being close to 1. Similarly, L is well correlated with both the magnetic energy E^b and the ohmic dissipation D^b although its instantaneous value involves the fluctuations of the velocity field. A weaker correlation is observed between the purely kinetic quantities and quantities involving the magnetic field: the amplitude of their cross correlation peaks at about 0.5. In addition, the correlation between the injected power and L and D^b decreases when the magnetic Prandtl number increases (see fig. 1(c), (d)). The source terms for kinetic (respectively, magnetic) energy are thus less correlated when Pm increases. The oscillations mostly visible in the correlation plot of fig. 1(b) are reminiscent of high frequency oscillations of the dynamo saturated in a given polarity.

Another feature is related to the sign of the extremum of the cross correlation function. It is positive among the quantities involved in the magnetic energy budget (eq. (4)), such that a fluctuation in the power of the Lorentz force is on average followed by a fluctuation with the same sign for both magnetic energy and ohmic dissipation. In contrast, it is followed by a fluctuation of the opposite sign for the injected power. Similarly, the kinetic and magnetic energies are anticorrelated, a decrease in magnetic energy being followed on average by an increase of kinetic energy.

One last information is provided by the time lags displayed by the correlation functions. It can be observed from $C^{PD^u}(\tau)$ that there is a time lag between injected

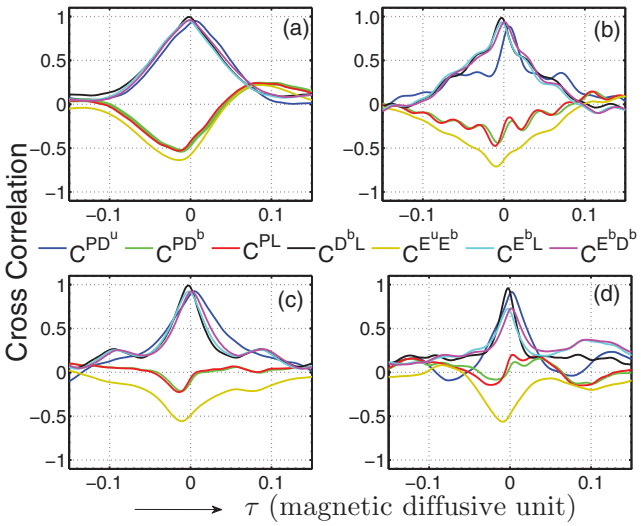

Fig. 1: Plot of the cross correlation $C^{XY}(\tau)$ *vs.* delay time τ for: (a) $Pm = 0.5$, $C = 1.5$ ($Rm_0 = 330$), (b) $Pm = 0.5$, $C = 2$ ($Rm_0 = 370$), (c) $Pm = 1$, $C = 2$ ($Rm_0 = 700$), and (d) $Pm = 2$, $C = 2$ ($Rm_0 = 1000$).

power and viscous dissipation (peak at positive delay time). This time lag is of the order of the large eddy turn-over time and corresponds to the time needed for the kinetic energy to cascade to dissipative scales, as often observed in turbulent flows [19]. Similarly, L, that is the source term for the magnetic energy, is slightly in advance compared to the magnetic energy and the ohmic dissipation. Less intuitive are the cross correlations that involve both kinetic and magnetic quantities. It is indeed observed that the power of the Lorentz force, magnetic energy and ohmic dissipation are all in advance compared to the injected power and the other kinetic quantities. The above results therefore suggest that the fluctuations of L are the ones that coherently affect the other energy transfers after some time lag. This can be understood since L couples kinetic and magnetic modes, thus its fluctuations are likely to affect the balance between kinetic and magnetic energy in a coherent way. Although it is clear from eqs. (3), (4) that a fluctuation of L will affect E^u and E^b in opposite ways, we however emphasize that it is not intuitive that the fluctuations of the kinetic energy lag the ones of the

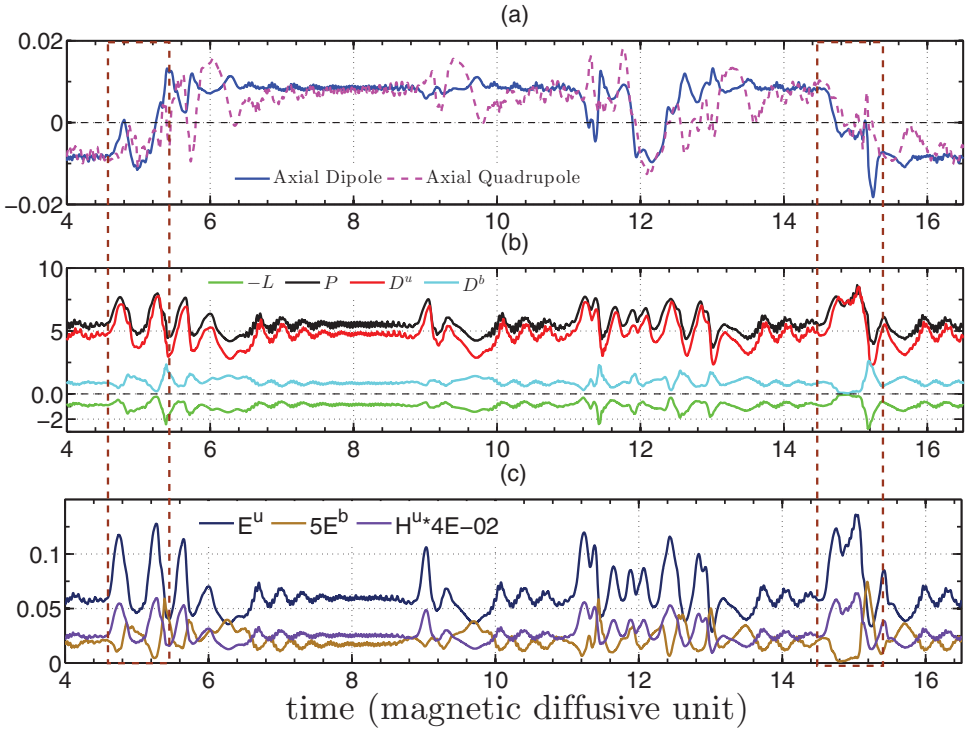

Fig. 2: Energy transfers for $Pm = 0.5$, and $C = 1.5$. Top panel: time series of axial dipole (blue) and quadrupole (pink). Middle panel: power of the Lorentz force L (green), injected power P (black), viscous dissipation D^u (red) and ohmic dissipation D^b (cyan). Bottom panel: kinetic energy E^u (black), magnetic energy E^b (brown) and kinetic helicity (purple).

magnetic energy. This may depend on the value of Pm (out of the range of the present study) or on the way the flow is forced. In the present simulation, the growth of magnetic energy is also followed by the decay of the flow kinetic helicity, $H^u = \langle \mathbf{u} \cdot (\boldsymbol{\nabla} \times \mathbf{u}) \rangle_V$, that displays a good correlation with E^u without time lag (see below).

The above results strongly suggest a precise chronology in the different energy flows during the magnetic field dynamics. In the following section, we therefore discuss their behavior during magnetic field reversals.

Energy transfers during dynamo reversals. – Figure 2 shows the temporal dynamics of the injected power P, dissipation rates (D^u and D^b), and power of the Lorentz force L for $Pm = 0.5$, and $C = 1.5$, when chaotic magnetic field reversals are observed. At the beginning of a reversal, as the amplitude of the axial dipole decreases, both L and D^b decrease. Since D^b stays larger than L, this phase is associated with a weakening of the magnetic energy.

On the contrary, in the kinetic equation, the injected power P and the viscous dissipation D^u both increase when the dipole vanishes. Since the net dissipation $D^u + L$ in the kinetic equation stays small compared to the total injected power, the kinetic energy thus increases during this period.

Once the dipole starts recovering its mean value, both L and D^b increase such that the magnetic energy grows. Viscous dissipation and injected power decrease in producing a net kinetic dissipation, *i.e.* $L + D^u$ is larger than the total injected power such that there is a decrease of the total kinetic energy during the recovery of the dipolar field.

The kinetic helicity H^u is shown in fig. 2(c). It is significantly smaller when the magnetic field is saturated in one polarity than during field reversals. Its fluctuations also display a clear anticorrelation with the ones of the magnetic energy E^b. As said above, H^u lags behind E^b, thus showing that the magnetic field inhibits the flow kinetic helicity. A similar mechanism has been put forward in mean-field dynamo models [20]. It seems to operate here although we have no scale separation.

Thus, for the simulations made at $Pm = 0.5$, the properties of the energy transfers inferred from the cross correlation functions computed on the whole time recordings can be observed on each individual reversal. The power of the Lorentz force decreases at the beginning of a reversal followed by the decrease of the magnetic energy or ohmic dissipation, whereas the injected power, the kinetic energy and then viscous dissipation first increase. In contrast to the kinetic and magnetic energies, the energy flows involve spatial derivatives of the velocity or magnetic fields. Thus, the fluctuations of viscous (respectively, ohmic) dissipation can be related to fluctuations of the amplitude of the velocity (respectively, magnetic) field and to change in their characteristic length scale. Consequently, it is not clear whether the decrease (respectively, increase) of ohmic (respectively, viscous) dissipation is primarily related to the decrease (respectively, increase)

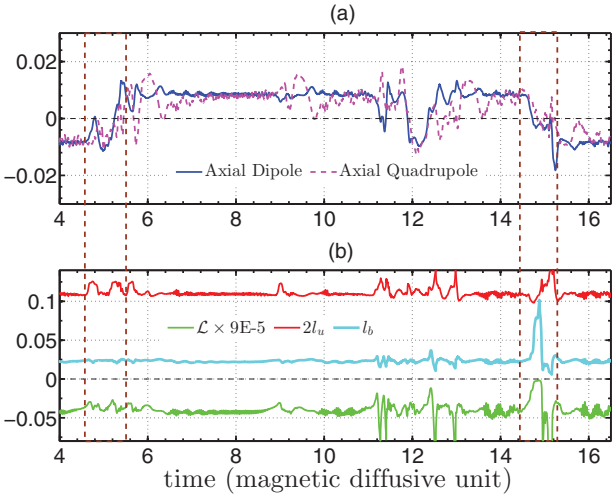

Fig. 3: Top panel: time series of axial dipole (blue) and axial quadrupole (pink). Bottom panel: time series of the normalized power of the Lorentz force $\mathcal{L}$ (green), effective velocity length scale l_u (red) and effective magnetic length scale l_b (cyan), for $Pm = 0.5$, and $C = 1.5$.

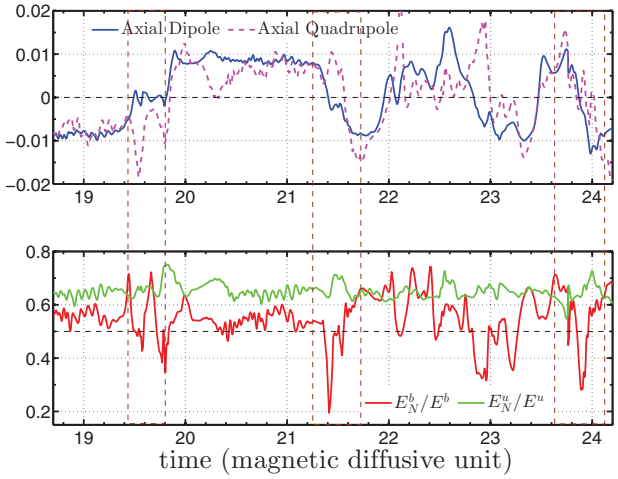

Fig. 4: Top panel: axial dipole (blue) and axial quadrupole (magenta) for $Pm = 0.5$ and $C = 1.5$. Bottom panel: time series of the relative kinetic energy in the northern hemisphere E_N^u/E^u (green) and of the relative magnetic energy in the northern hemisphere E_N^b/E^b (red).

of the magnetic (respectively, kinetic) energy. This is also true for $L = -Rm_0\langle \mathbf{u}\cdot[(\boldsymbol{\nabla}\times\mathbf{b})\times\mathbf{b}]\rangle_V$, that can be also written $L = -Rm_0\langle(\partial_i u_j + \partial_j u_i)b_i b_j\rangle_V/2$ if the flow is incompressible. An additional feature of L is its dependence on the respective angles between the different fields. In order to get further insight in the fluctuations of the energy transfers during reversals, we normalize the viscous (respectively, ohmic) dissipation by the kinetic (respectively, magnetic) energy, by computing the quantities $l_u = [D^u/E^u)]^{-1/2}$ and $l_b = [D^b/E^b]^{-1/2}$. In addition we also define the normalized power of the Lorentz force as $\mathcal{L} = L/\sqrt{D^u}E^b$. Note that these normalized dissipations can be regarded as changes in the kinetic (respectively, magnetic) length scale, while $\mathcal{L}$ involves some correlation between local dissipation and the magnetic field. Figure 3 displays these quantities. The velocity length scale increases when reversals occur and strongly decreases during the dipole overshoot. The behavior of the magnetic length scale and of $\mathcal{L}$ displays more variability from one reversal to the other. This results from the variability of the minimum magnetic energy achieved during reversals (see fig. 2(c)).

The characteristic features displayed by the energy transfers during field reversals for $Pm = 0.5$ are not observed for Pm larger ($Pm = 1$ or 2). Neither the kinetic (respectively, magnetic) energy nor the different energy flows display some systematic changes during reversals compared to regimes of given polarity (data not shown). The effect of Pm on the reversal mechanism has been emphasized in previous studies [14]: it has been shown that the reversals obtained at $Pm = 0.5$ primarily involve the coupling of the axial dipole with an axial quadrupole in the framework of a simple model [13] whereas more modes generate dynamics with more variability for reversals observed at larger Pm.

Drift of the magnetic energy during field reversals. – It has been recently reported in the VKS experiment that a spatial localization of the dynamo magnetic field occurs when the symmetry of the driving is broken by rotating the two propellers at slightly different velocities [21]. In addition, it has been observed that the maximum of magnetic energy drifts during a field reversal. It crosses the equatorial plane and comes back to its initial location at the end of the reversal. These phenomena could be related to hemispherical dynamos observed in some planets or stars. The present numerical simulations provide a convenient tool to study hemispherical dynamos and the spatiotemporal dynamics of the magnetic field during reversals. To wit, we compute the kinetic (respectively, magnetic) energy in the northern hemisphere E_N^u (respectively, E_N^b) by integrating the kinetic (respectively, magnetic) energy density restricted to the northern hemisphere. The kinetic (respectively, magnetic) energy fraction in the northern hemisphere E_N^u/E^u (respectively, E_N^b/E^b) during field reversals is displayed in fig. 4. We observe that E_N^u/E^u is significantly larger than 0.5 because the flow forcing is stronger in the northern hemisphere ($C = 1.5$). The magnetic field is also on average stronger in the northern hemisphere. However, E_N^b/E^b drops significantly below 0.5 during field reversals. Thus, the maximum of magnetic energy density migrates from the northern to the southern hemisphere during a field reversal and then comes back to its initial location after the reversal.

Some differences with the VKS experiment should be mentioned: in the experiment, the magnetic energy is stronger close to the slow propeller when the speeds are slightly different. It becomes localized close to the fast propeller, similarly to the present simulations, only when

the rotation speeds significantly differ. In addition, the asymmetry in the distribution of the magnetic energy density in the experiment looks stronger than in the simulations. This can be related to the difference of thresholds of the dipolar and quadrupolar modes [21,22]. Reversals in the VKS experiment can be superimposed whereas they display a much stronger variability in the present numerical simulations, even at the lowest value of Pm. This is related to the stronger contribution of modes higher than the dipolar and quadrupolar ones in the simulation. Despite these higher modes, the diagnostic provided by the recording of E_N^b/E^b during reversals is rather robust when Pm is small enough and the migration of the maximum magnetic energy density through the equatorial plane during reversals is in agreement with the experimental observations.

Conclusion. – We have studied the properties of energy transfers and their correlations in fluctuating dynamo regimes involving field reversals. Cross correlation functions show that fluctuations of the power L of the Lorentz force are in advance with respect to fluctuations of ohmic and viscous dissipation as well as magnetic or kinetic energy. Somewhat surprisingly, kinetic quantities lag behind the magnetic ones. This is true for kinetic energy and viscous dissipation but also for kinetic helicity that displays fluctuations opposite to the ones of magnetic energy. This does not mean that the reversal cannot be triggered by changes in the flow regime. Changes in the flow regime may result in significant changes of L, but which could make very little difference to the kinetic quantities. However, fluctuations of L can be also related to changes in the magnetic field or to geometrical properties such as the distribution of the angle between the velocity and the magnetic (respectively, current density) field. The dominant mechanism is likely to depend on the value of Pm. This deserves further studies.

Another observation presented here that deserves to be checked in other dynamos is the anticorrelation of the magnetic and kinetic energy fluctuations. This trend would be obvious for systems at equilibrium with a constant total energy but dynamos are not expected to operate in such a regime since injected power and dissipation strongly affect the energy budget of these out-of-equilibrium systems. It would be of interest to check whether this trend is observed in most turbulent dynamos at high Re and Rm.

* * *

Support of IFCPAR/CEFIPRA contract 4904-A is acknowledged.

REFERENCES

[1] Brunhes B., *J. Phys. Theor. Appl.*, **5** (1906) 705.
[2] Roberts P. H. and Glatzmaier G. A., *Rev. Mod. Phys.*, **72** (2000) 1081.
[3] For a review, see Pétrélis F. and Fauve S., *Philos. Trans. R. Soc. A*, **368** (2010) 1595.
[4] Parker E. N., *Astrophys. J.*, **158** (1969) 815.
[5] Parker E. N., *Cosmical Magnetic Fields* (Clarendon Press, Oxford) 1979.
[6] Sarson G. R. and Jones C. A., *Phys. Earth Planet. Inter.*, **111** (1999) 3.
[7] Glatzmaier G. A. and Roberts P. H., *Nature*, **377** (1995) 203.
[8] Wicht J. and Olson P., *Geochem. Geophys. Geosyst.*, **5** (2004) Q03H10.
[9] Aubert J., Aurnou J. and Wicht J., *Geophys. J. Int.*, **172** (2008) 945; Olson P. L., Glatzmaier G. A. and Coe R. S., *Earth Planet. Sci. Lett.*, **304** (2011) 168.
[10] Busse F. H. and Simitev R., *Geophys. Astrophys. Fluid Dyn.*, **304** (2006) 341; Kutzner C. and Christensen U. R., *Phys. Earth Planet. Inter.*, **131** (2002) 29.
[11] Li J., Sato T. and Kageyama A., *Science*, **295** (2002) 1887; Nishikawa N. and Kusano K., *Phys. Plasma*, **15** (2008) 082903; Gissinger C. *et al.*, *Phys. Rev. Lett.*, **108** (2012) 234501.
[12] Berhanu M. *et al.*, *EPL*, **77** (2007) 59001.
[13] Pétrélis F. and Fauve S., *J. Phys.: Condens. Matter*, **20** (2008) 494203; Pétrélis F. *et al.*, *Phys. Rev. Lett.*, **102** (2009) 144503.
[14] Gissinger C., Dormy E. and Fauve S., *EPL*, **90** (2010) 49001.
[15] Bayliss R. A. *et al.*, *Phys. Rev. E*, **75** (2007) 026303.
[16] Gissinger C., Dormy E. and Fauve S., *Phys. Rev. Lett.*, **101** (2008) 144502.
[17] Dormy E., PhD Thesis (IPGP, Paris) 1997; Dormy E. *et al. Earth Planet. Sci. Lett.*, **160** (1998) 15.
[18] Buffet B. A. and Bloxham J., *Geophys. J. Int.*, **149** (2002) 211.
[19] Lumley J. L., *Phys. Fluids A*, **4** (1992) 203.
[20] Cattaneo F. and Hughes D. W., *Phys. Rev. E*, **54** (1996) R4532.
[21] Gallet B. *et al.*, *Phys. Rev. Lett.*, **108** (2012) 144501.
[22] Gallet B. and Pétrélis F., *Phys. Rev. E*, **80** (2009) 035302.